Predicting *in vivo* fluorescence lifetime behavior of near-infrared fluorescent contrast agents using *in vitro* measurements

Walter J. Akers
Mikhail Y. Berezin
Hyeran Lee
Samuel Achilefu
Washington University School of Medicine
Optical Radiology Laboratory
Department of Radiology
4525 Scott Avenue
Saint Louis, Missouri 63110

Abstract. Fluorescence lifetime (FLT) information is complementary to intensity measurement and can be used to improve signal-to-background contrast and provide environment sensing capability. In this study, we evaluate the FLTs of eight near-infrared fluorescent molecular probes *in vitro* in various solvent mediums and *in vivo* to establish the correlation between the *in vitro* and *in vivo* results. Compared with other mediums, two exponential fittings of the fluorescence decays of dyes dissolved in aqueous albumin solutions accurately predict the range of FLTs observed *in vivo*. We further demonstrate that the diffusion of a near-infrared (NIR) reporter from a dye-loaded gel can be detected by FLT change in mice as a model of controlled drug release. The mean FLT of the NIR probe increases as the dye diffuses from the highly polar gel interior to the more lipophilic tissue environment. The two-point analysis demonstrates an efficient *in vitro* method for screening new NIR fluorescent reporters for use as FLT probes *in vivo*, thereby minimizing the use of animals for FLT screening studies. © *2008 Society of Photo-Optical Instrumentation Engineers.*
[DOI: 10.1117/1.2982535]

1 Introduction

Optical detection methods using organic fluorescent contrast agents are widely used in biomedical research from *in vitro* assays and microscopy to whole-animal preclinical imaging.[1] While steady-state fluorescence imaging (intensity versus wavelength) is frequently used as an optical detection technique, time-resolved fluorescence measurements are becoming popular in biological research because of advances in imaging techniques and increased commercial availability of economical lasers and electronic components.[2–4] Fluorescence lifetime (FLT) is an intrinsic property of fluorescent compounds and corresponds to the average amount of time the molecules spend in the excited state prior to emission of a photon. An advantage of FLT imaging lies in the high sensitivity of the FLT properties of organic dyes to their environment such as pH, polarity, viscosity, oxygen saturation, or protein binding. The insensitivity of FLT on the local dye concentration minimizes the detrimental effects of concentration artifacts, including photobleaching and dye decomposition. In addition, the FLT is less perturbed by light scattering,[5,6] excitation intensity, or sample turbidity.[7] FLT imaging also allows multiplex resolution of probes that exhibit the same steady-state optical properties (absorption and emission) with different FLT characteristics. Thus, multiple targeted agents can be resolved within the same living biological system that allows monitoring diverse physiological processes at the same time. Current instrumentation allows FLT resolution of less than 0.2 ns, which favors detection of small FLT changes.

FLT imaging microscopy and FLT endoscopy have utilized intrinsic tissue FLT data to assess differences in distribution of factors such as NADH and FADH and their oxidation state to correlate with pathologic changes or other biological processes.[8] In addition, FLT-sensitive fluorescent probes with light emission below 600 nm have been developed for more accurate sensing of oxygen, calcium, and pH.[4] Although these probes may be adequate for cell studies, their relatively short emission wavelength confines their use to studies where the depth of light penetration is not a concern. Previous studies have shown that molecular probes that absorb and emit light in the near-infrared (NIR) range (700 to 900 nm) are best suited for *in vivo* imaging. Accordingly, our laboratory and others initiated studies to explore the potential of FLT imaging using NIR molecular probes in whole-animal optical imaging.[9–15] For example, we recently showed subtle FLT differences in mouse tumor versus liver using a NIR tumor-specific agent[10] and demonstrated the use of the same excitation and emission parameters to separate signals from two different NIR molecular probes in an *in vivo* animal model.[9] The increased use of contrast-enhanced FLT imaging has

Address all correspondence to: Samuel Achilefu, Optical Radiology Lab, 4525 Scott Avenue, St. Louis, MO 63110; Tel: 314-362-8599; Fax: 314-747-5191; E-mail: achilefus@mir.wustl.edu

prompted the need to adequately characterize the FLT properties of existing and new NIR fluorescent probes. Our previous study shows that NIR polymethine cyanine dyes, which are widely used for *in vivo* studies, have small but distinct FLT changes in mediums with different solvent polarity index.[16] Considering the heterogeneity within living tissues, similar FLT changes are expected in animals.

To minimize the number of animals used to screen the behavior of the FLT properties of these dyes *in vivo*, we explored the correlation of FLT changes *in vitro* with *in vivo* data. This allowed development of a high throughput *in vitro* model to predict the behavior and to sense normal and abnormal physiological by FLT changes *in vivo*. The FLTs of NIR probes in various solvents with different polarity index were compared to the *in vivo* data to develop a scale of FLT sensitivity. We found that the mean FLT in aqueous albumin solution was close to the maximum value of the FLT *in vivo*, while the minimum value was close to polar solutions such as water. We further demonstrated the utility of FLT imaging in a controlled drug-release model that releases a polymethine dye (cypate) from a gel. The measured mean FLT of cypate reflected the differences of environment polarity between the gel and mouse tissue.

2 Methods

2.1 Near-Infrared Imaging Agents

Near-infrared dyes indocyanine green (ICG), IR-820, IR-806, and 3,3′-diethylthiatricarbocyanine iodide (DTTCI) were purchased from Sigma-Aldrich (Saint Louis, Missouri) and used without further purification. Cypate, LS-276, LS-277, and LS-288 were synthesized as described previously,[17–19] and their photophysical properties were described elsewhere.[16,20] Bovine serum albumin (BSA) was obtained from Sigma-Aldrich. Methanol, ethanol, acetone, dimethylsulfoxide (DMSO), methylene chloride (DCM), and chloroform were of spectroscopic grade quality and ultrapure water (Milli-Q, Millipore, Billerica, Massachusetts) was used throughout the study.

2.2 In Vitro Spectroscopic Measurements

BSA (50 mg) was dissolved in 1 mL of 0.01-M phosphate-buffered saline (PBS, Sigma-Aldrich) to obtain physiologic-relevant concentration of albumin in human plasma. The stock solutions of the dyes (50 to 100 μM) in DMSO were stored at $-20\,^\circ$C in the dark. Aliquots were added to the appropriate solvents or BSA-PBS solution (1 mL) and vortexed for 1 min. To prevent an inner filter effect, samples were further diluted with the appropriate organic solvent or PBS buffer to adjust the absorbance maximum between 0.1 and 0.3.

Absorbance spectra were recorded on a Beckman Coulter DU 640 spectrophotometer (Fullerton, California) and fluorescence steady-state spectra were recorded on a Fluorolog III fluorometer (Horiba Jobin Yvon, Edison, New Jersey) with 720-nm excitation and 5-nm band slits. All measurements were conducted at room temperature. The FLTs were measured using a time-correlated single-photon-counting (TCSPC) technique (Horiba) with 773-nm excitation source NanoLed® (impulse repetition rate 1 MHz) at 90 deg to the detector (Hamamatsu Photonics, Japan). For the FLT measurements, the absorbance of the working solutions was maintained below 0.15 at 773-nm excitation wavelength by dissolving the stock solutions in the appropriate solvents. The FLT of cypate-agarose gel was recorded in solid state using a solid sample holder at about 45 deg to the path of light beam to avoid direct light reaching the detector. The angle was optimized with a blank agarose gel without cypate. The detector was set to 820 nm with a 20-nm bandpass. The electrical signal was amplified by a TB-02 pulse amplifier (Horiba) fed to the constant fraction discriminator (CFD, Phillips, The Netherlands). The first detected photon was used as a start signal by a time-to-amplitude converter (TAC), and the excitation pulse triggered the stop signal. The multichannel analyzer (MCA) recorded repetitive start-stop signals from the TAC and generated a histogram of photons as a function of time-calibrated channels (6.88 ps/channel) until the peak signal reached 10,000 counts. The FLT was recorded on a 50-ns scale. The instrument response function was obtained using a Rayleigh scatter of Ludox-40 (0.03% in MQ water; Sigma-Aldrich) in a quartz cuvette at 773-nm emission. Decay analysis software (DAS6 v6.1, Horiba) was used for FLT calculations. The goodness of fit was judged by χ^2 values, Durbin–Watson parameters, as well as visual observations of fitted line, residuals, and autocorrelation functions. Two-exponential analyses were normally used for data fitting, except where three-exponential decay equations were used to improve χ^2 for analysis in BSA solutions. When the FLT components with insignificant contribution ($<3\%$) were discarded, the decays were reported as single- or dual-component systems in the case of a two- or three-exponential fit. For solution systems with two emitting species, such as the BSA solutions, the FLTs were calculated by the following equations:

$$I(t) = \sum_{i=1}^{n} A_i \exp(-t/\tau_i), \tag{1}$$

$$F_i = \frac{A_i \tau_i}{\Sigma_i A_i \tau_i}, \tag{2}$$

where F_i is the fractional component (percent), τ_i is the FLT (ns), A_i is the amplitude, and n is 2 for the two-exponential model. Fitting of fluorescence decays with a single exponential model ($n=1$) was used to report the average FLT.

2.3 Animal Treatment

All animal studies were performed in compliance with the Washington University School of Medicine Animal Studies Committee requirements for the humane care and use of laboratory animals in research. For *in vivo* NIR probe FLT measurement, male NCR nude mice were anesthetized and maintained with isoflurane gas (2% v/v) for fluorescent agent administration and imaging. Contrast agents dissolved in 100 μL of 20% DMSO were injected via lateral tail vein. Concentrations were based on absorbance at 780 nm, equivalent to 60-μM cypate. For imaging of subcutaneously implanted cypate-loaded agarose gels, mice were anesthetized and maintained with isoflurane gas (2% v/v). A 5-mm incision was made through the skin flank region and a pocket made in the subcutaneous tissue by blunt dissection. A
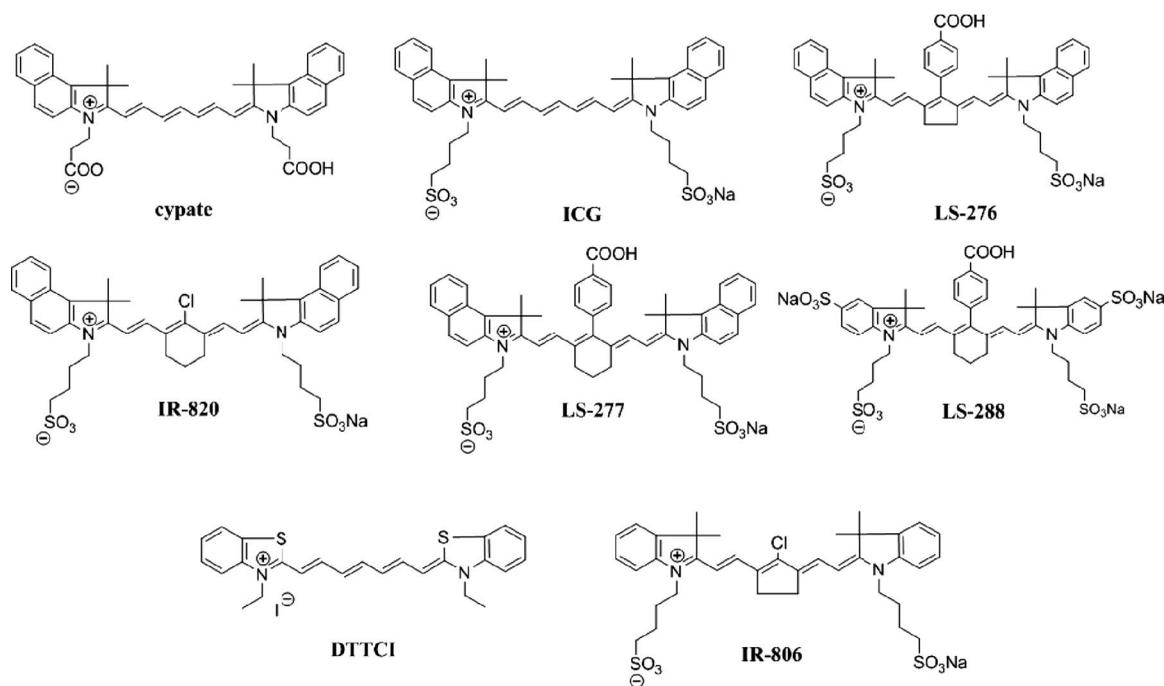
Fig. 1 Chemical structures of NIR fluorescent dyes used in this study.

0.5-mm^3 slab (1×1-mm square by 0.5 mm thick) of 1% agarose gel containing 60-μM cypate was inserted into the pocket and the incision was closed with tissue adhesive. Gels were positioned such that the incision lay on the lateral aspect, with uninterrupted skin over the gel surface.

2.4 *Imaging Method and Analysis*

In vivo mouse images were acquired with a time-domain diffuse optical imaging system (eXplore Optix, ART, Incorporated, Montreal, Canada). The system produced excitation light via a 780-nm, 80-MHz pulsed diode laser and captured emitted photons by fast photomultiplier tube with an 830-nm telecentric emission filter. The detection system included a time-correlated single-photon counting device for *in vivo* fluorescence decay recording. The focal points of excitation and emission detection were separated by 3 mm to detect diffusely scattered fluorescence photons. Diffuse optical imaging improves depth resolution relative to reflectance imaging.[21] FLT imaging in live mice was performed as reported previously.[9,10] Briefly, the animals were positioned on the heated imaging platform and a 2-D scanning region of interest (ROI) was selected by a top-view charge-coupled device (CCD) camera to include the area from the neck to the pelvis. The 780-nm pulsed diode laser was set to 0.4 μW for excitation scans and adjusted for optimal signal strength, in the range 5 to 70 μW for fluorescence detection. ROI were raster scanned in 1.5-mm increments for the controlled drug release (CDR) model and 3-mm increments for the contrast agent imaging with 0.3-s integration time per pixel. Fluorescence data were acquired 0.5 to 2.5 h after agent injection. Acquired images were analyzed with the OptiView software provided by ART. Data were reported as fluorescence intensity or FLT maps, with each pixel representing the integration or curve fitting of the acquired temporal point-spread function

(TPSF), respectively, at each detection point. Pixels with less than 1×10^5 photon counts per second were not included in the FLT measurement due to insufficient signal. *In vivo* FLT maps are displayed after fitting a single exponential decay function for simplicity. To determine the best model for *in vivo* FLT results, FLT values from different solvent models were compared to the average FLT values in the liver region from *in vivo* imaging. The liver region was chosen for data sampling, as most agents accumulated in this organ nonspecifically relative to other tissues.

2.5 *Statistical Analysis*

Column statistics were performed to assess the correlation of *in vitro* and *in vivo* FLT measurements. Percent differences were calculated for each *in vitro* model relative to the reference model to assess the ability of each solvent system to predict *in vivo* FLT behavior. The percent differences were compared to assess the agreement of each *in vitro* model in relation to the *in vivo* FLT measurements. All analyses were performed using Prism 4.0 (GraphPad Software, San Diego, California).

3 Results

3.1 *Chemistry*

NIR molecular probes synthesized in our laboratory and from commercial sources used in this study are shown in Fig. 1. All compounds are based on heptamethine dyes that differ in the nature of the heterocyclic end groups or substituents at the mesoposition. The linear heptamethine dye cypate was prepared in high yield ($>60\%$) from the reaction of glutaconaldehyde and the propanoic acid derivative of benzoindole, as reported previously.[17,22] The mesosubstituted dyes were prepared by a modified Suzuki coupling method.[18] The purity of

Table 1 FLTs (ns) of NIR molecular probes measured in various solvents and after intravenous administration in living mice. Data were fitted by a single exponential decay model. Standard deviations (sd) were less than 5% for *in vitro* measurements.

	Chloroform	DCM	DMSO	Acetone	Ethanol	Methanol	Water	Albumin	*In vivo* ±sd
LS-288	N/A	N/A	1.33	1.02	1.00	0.81	0.44	1.00	1.12±0.02
LS-276	1.25	1.17	1.11	1.13	0.87	0.83	0.36	0.88	1.12±0.01
DTTCI	1.82	1.72	1.49	1.54	1.21	1.07	0.49	1.14	1.04±0.01
IR-806	1.28	1.15	1.01	1.02	0.82	0.66	0.27	0.61	0.77±0.02
LS-277	1.62	1.34	0.98	0.84	0.69	0.61	0.2	0.78	0.74±0.00
ICG	1.14	0.91	0.97	0.87	0.62	0.51	0.17	0.79	0.69±0.01
Cypate	1.01	0.94	0.87	0.8	0.57	0.46	0.2	0.62	0.63±0.00
IR-820	0.73	0.59	0.50	0.43	0.38	0.25	0.13	0.49	0.53±0.02

all prepared compounds was determined by HPLC and LC-MS analyses. The choice of the dyes was based on several criteria. First, the dyes were selected to represent a broad range of FLTs from 0.49 ns for IR-820 to 1.14 ns for DTTCI in albumin. Second, the probes were selected to represent different degrees of hydrophilicity determined by a number of sulfate groups in the molecule. For example, cypate with no sulfonate groups was sparingly insoluble in water, while LS-288 with four sulfonate groups was highly water soluble. Third, the synthesized dyes were designed to possess a reactive functionality (here, the carboxylic acid group) for labeling biomolecules such as peptides and proteins.

3.2 Comparison of In Vitro and In Vivo Fluorescence Lifetimes of Molecular Probes

The spectral properties of the dyes were determined in solvents with different solvent polarity to explore the FLT behavior in different environments, as reported previously.[16] In these solvents, all of the dyes absorbed and emitted light in the NIR region (700 to 900 nm). The dyes also exhibited relatively small bathochromic absorption and emission shifts (5 to 30 nm) in high polarity relative to low polarity solvents, which is typical of heptamethine dyes.[16] In contrast, the dynamic emission spectra show significant solvent-dependent changes in FLT values. The FLT changes correlated with the solvent polarity function, such as solvent orientation polarizability Δf. In general, the FLT showed a decrease from low to high polarity solvents (from low to high values of Δf). The fluorescence decays in most solvents were monoexponential (>95% fractional contribution from the major component constituted the two exponential analysis), suggesting the presence of one major form of the emitter in solution (Table 1). This indicates the homogeneity of the solutions, albeit with polarity-dependent FLTs in different solvents.

We also examined the FLT properties of the dyes in albumin, a major transport protein in blood. The average FLTs of single-exponential decay fits are shown in Table 1. According to molecular modeling studies,[20] albumin offers at least two binding pockets with significantly different polarities for the

binding of heptamethine molecules. As a result, the molecular probes bound to albumin could exist in two different microenvironments that exhibit two distinct FLTs with corresponding fractional contributions. In contrast to the single exponential decays found in organic solutions, the fluorescence decays in albumin solutions show a two-exponential decay, revealing the presence of the two light-emitting states, except for DTTCI (Table 2).

For *in vivo* FLT study, mice were imaged after intravenous injection of individual dyes. The resulting FLT maps of the dyes were relatively flat compared with the intensity images, indicating the poor dependence of FLT on the dye concentration (Fig. 2).

Each compound tested demonstrated relatively distinct FLTs ranging from 0.53 to 1.12 ns. The mean *in vivo* FLTs measured from the liver region for different dyes are shown in Table 1 and reflect the general trend that fluorescent probes with longer FLTs *in vitro* in any given solvent typically show longer FLT *in vivo*. An exception to the relatively flat FLT trend is the heterogeneous fluorescence intensity and FLT maps of LS-288 in mice (Fig. 3). The distinct short FLT in the bladder (0.70 ns) relative to other parts of the body (1.12 ns) was observed, indicating the water-rich environment in the urine (Table 3). The hydrophilic characteristics of the dye resulted in significant renal clearance relative to the more hydrophobic dyes used in this study.

Our results show that the dye FLTs in albumin solutions best approximates the *in vivo* range of FLT as measured from the liver region. A graphical box and whiskers plot of this analysis is shown in Fig. 4. Two-exponential fitting of the acquired TPSFs for dyes in albumin solutions reliably predicted the range of FLTs observed *in vivo*, with the largest deviations from the mean (monoexponential fitting) *in vivo* measurements apparently due to differences in protein binding fractions (Table 2). FLT values for compounds in aqueous albumin solution showed the lowest bias relative to other solvents with an average difference of 0.7%.

Table 2 Measured two-component FLT (τ, ns) of dyes from albumin solutions compared with FLTs in the liver region in mice after intravenous administration. Good agreement was observed between the two FLT components *in vitro* and *in vivo*. The *in vitro* and *in vivo* fractional composition of FLTs in the liver were significantly different for LS-276 and DTTCI, indicating the differences in protein-binding characteristics of the molecular probes. Standard deviations for *in vitro* measurements were less than 5%. *In vitro* τ_1 (F_1) is a fractional component (%); and NS is for not significant.

| | In vitro | | In vivo | |
Compound	τ_1 (F_1)	τ_2 (F_2)	τ_1 (F_1)	τ_2 (F_2)
LS-276	0.69 (55)	1.19 (42)	0.77±0.06 (14)	1.16±0.02 (86)
DTTCI	NS	1.14 (95)	0.34±0.03 (30)	1.12±0.02 (70)
IR-806	0.52 (60)	1.19 (38)	0.45±0.02 (62)	1.04±0.04 (38)
LS-277	0.64 (65)	1.15 (32)	0.48±0.03 (63)	0.98±0.02 (37)
Cypate	0.47 (69)	0.97 (30)	0.41±0.01 (75)	0.96±0.01 (25)
ICG	0.63 (61)	1.10 (37)	0.53±0.02 (67)	0.90±0.02 (33)
IR-820	0.41 (77)	0.91 (19)	0.41±0.02 (85)	0.92±0.02 (15)

3.3 Agarose Gel Implant Fluorescence Lifetime Imaging

Having demonstrated the potential to predict the *in vivo* behavior of NIR dyes in various mediums, we explored the use of FLT changes to monitor the release of encapsulated dyes *in vivo*. We used agarose gel implant containing cypate as a model of controlled drug release for this study. The site of surgery did not swell or show significant signs of inflammation during the imaging period, nor did the mice show signs of irritation or pain from the implant. High fluorescence intensity was measured from the area of the gel implant with significant fluorescence detected from the area surrounding the gel. We also detected fluorescence from the contralateral liver and kidney regions by 3-h postimplant, demonstrating rapid cypate
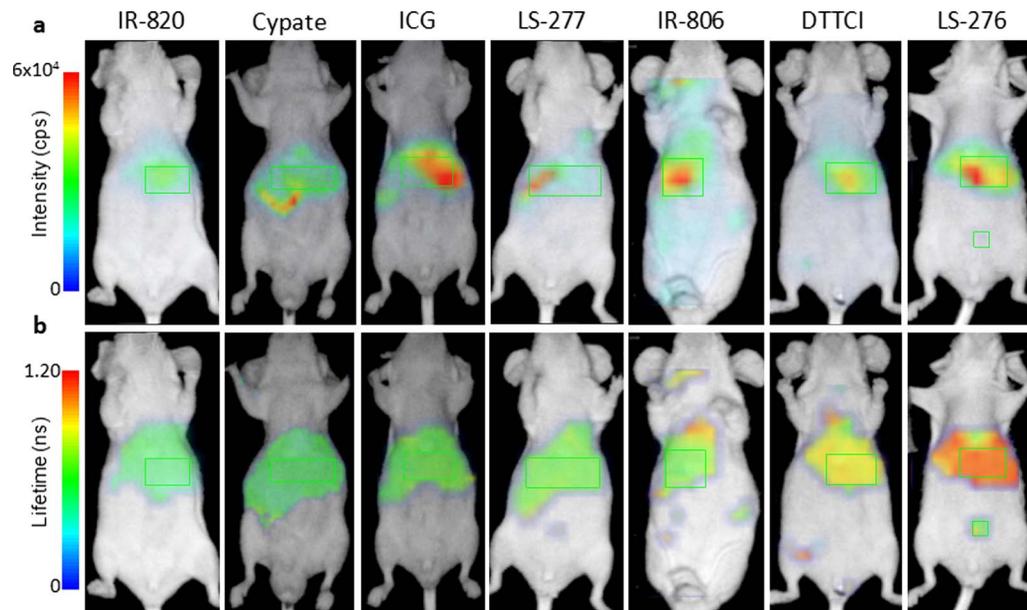

Fig. 2 (a) *In vivo* fluorescence intensity and (b) FLT ventral aspect image maps of mice injected with NIR fluorescent dyes 1 to 4 h postinjection. FLT maps were created from TPSF data acquired using the time-domain diffuse optical imaging system. FLT measurements were selected from the liver region (green rectangles) based on high fluorescence intensity and anatomical location for comparison to minimize discrepancies in organ distribution, as all dyes showed evidence of hepatobiliary elimination. Some of the dyes showed partial renal clearance with fluorescence signal from the bladder (indicated by abdominal ROI for LS-276). The collected signal was insufficient for accurate FLT measurement from the bladder for these specimens. Differences in the positions of the liver and kidney regions in different animals are due to the shifting of these internal organs in animals. (Color online only.)
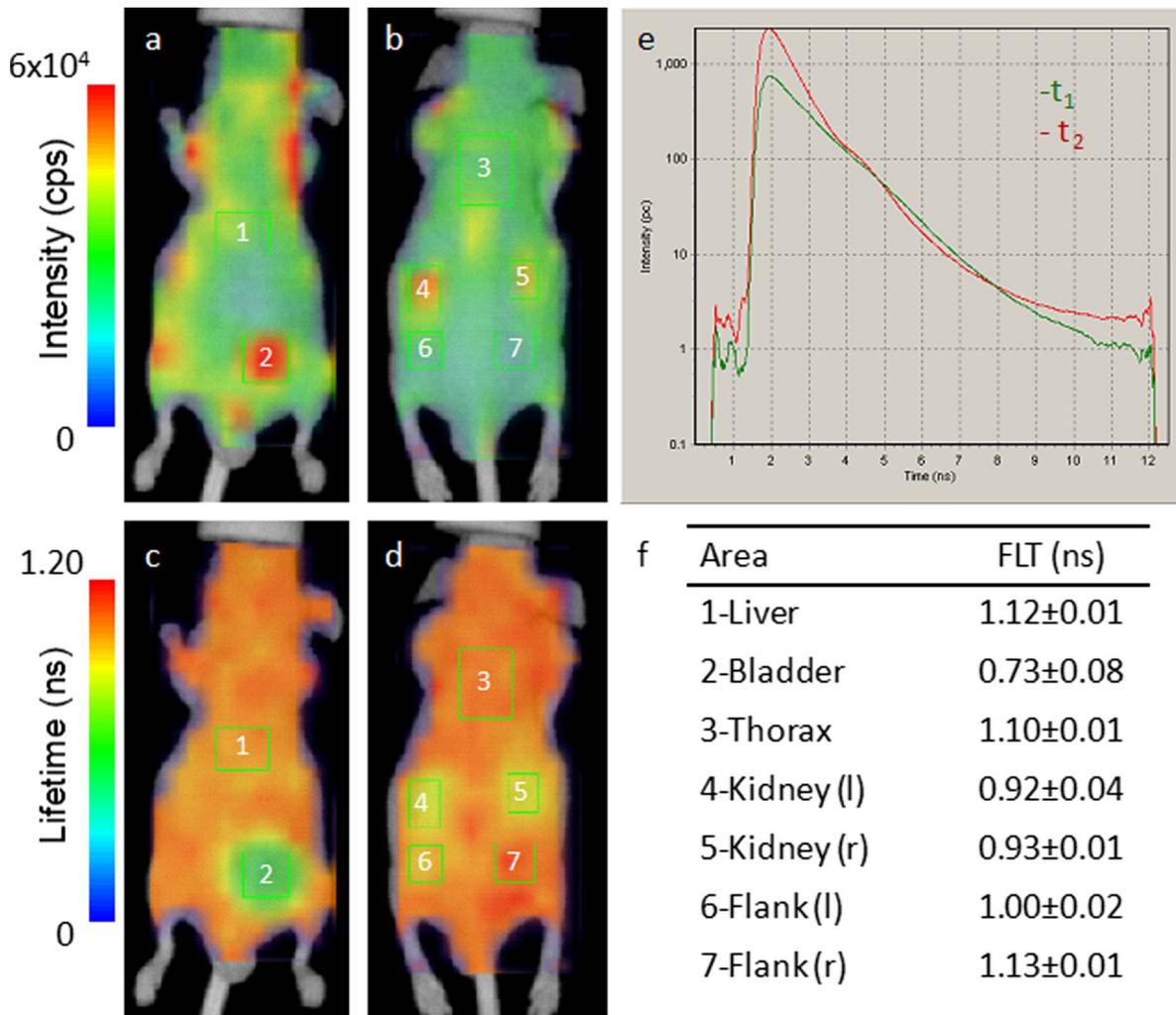
Area	FLT (ns)
1-Liver	1.12±0.01
2-Bladder	0.73±0.08
3-Thorax	1.10±0.01
4-Kidney (l)	0.92±0.04
5-Kidney (r)	0.93±0.01
6-Flank (l)	1.00±0.02
7-Flank (r)	1.13±0.01

Fig. 3 *In vivo* fluorescence intensity (a) ventral and (b) dorsal and FLT maps (c) ventral and (d) dorsal of nude mouse 2 h after intravenous injection of LS-288 solution. The FLT distribution is heterogeneous with distinctly different FLTs observed in the bladder and kidneys relative the rest of the body. Representative fluorescence TPSFs for the liver (1) and bladder (2) ROIs are shown in (e) and demonstrate the dominance of the long-FLT component in the liver and the short-FLT component in the bladder (multiexponential fitting data in Table 2). The mean detected FLT from each ROI is presented in (f), which compares favorably with the expected water-rich environment in urine. ROI 6 corresponds to the dorsal aspect of ROI 2 (bladder), indicating that the short FLT relative to ROI 7 is due to muscle tissue overlying ROI 2 in this position. A tomographic method could be used to isolate the contribution of adjacent tissues to the FLT.

diffusion and absorption into systemic circulation [Fig. 5(a)]. The measured FLT in the tissue surrounding the gel was substantially higher at several millimeters from the gel relative to the FLT of cypate in the agarose gel [Fig. 5(b)] with a near linear increase over distance from the gel center [Fig. 5(c)]. Because cypate is cleared from the body through the hepatobiliary pathway, it is also possible that the stomach and intestines contributed some of the detected fluorescence in the liver and kidney regions.

4 Discussion

FLT imaging is a versatile approach to study physiological and molecular processes.[23–30] The *in vivo* applications of FLT imaging using exogenous molecular probes require a clear understanding of the *in vivo* FLT properties of various dyes to delineate imaging artifacts from real signals. This is particularly important when using exogenous contrast agents capable of altering their FLTs. Although the FLT properties of many visible fluorescent proteins and dyes are well documented, those of NIR molecular probes are not readily available. Recently, our laboratory and others have mapped the FLTs of NIR dyes in animals.[9,10,14] In one study, we showed that the FLT of a tumor-specific molecular probe exhibited small FLT differences in the tumor and the liver.[10] A more recent study demonstrated our ability to separate the distribution of two NIR fluorescent probes in the same animal based on their FLTs.[9] Other laboratories have developed a tomographic approach for high resolution FLT imaging in small animals.[11,13,31] With the availability of these instruments and diverse NIR molecular probes, it is only a matter of time before a surge in their *in vivo* use becomes a reality.

However, minimization of the number of animals needed to evaluate the FLT properties of new molecular probes *in vivo* would be facilitated by developing an *in vitro* model to

Table 3 Measured FLTs (τ, ns) of LS-288 *in vitro* and *in vivo* comparing the protein-bound fractions in albumin solution and in the liver ROI to that of relatively water-rich urine. Standard deviations were less than 5% for *in vitro* measurements.

	In vitro			In vivo	
	τ_1 (F_1)	τ_2 (F_2)		τ_1 (F_1)	τ_2 (F_2)
Albumin	0.61 (37)	1.29 (60)	Liver	0.65±0.06 (29)	1.23±0.03 (71)
Urine	0.42 (82)	0.99 (15)	Bladder	0.48±0.02 (75)	1.09±0.05 (25)

predict the FLT properties of these dyes. We recently demonstrated the high sensitivity of the FLTs to the polarity of the mediums for heptamethine NIR fluorescent probes.[16] There are four major decay pathways for these cyanine dyes from the singlet excited state to the ground state: 1. radiative fluorescence process and three nonradiative pathways that include 2. internal conversion, 3. intersystem crossing, and 4. photoisomerization. Generally, a photoisomerization decay pathway is solvent dependent, while the internal conversion is a solvent-independent process. Polar solvents facilitate the mobility of the bonds in the excited state, diverting the energy from radiative to nonradiative pathways that result in shorter FLT. Although we established a correlation between the solvent polarity function and FLT by determining the dye FLTs in various solvents, a correlation between *in vitro* and *in vivo* data is required to help interpret *in vivo* FLT images. This calls for the development of an *in vitro* system for high throughput screening of NIR probes for *in vivo* use, thereby minimizing the number of animals used for such screening studies.

Although many factors could affect FLTs, we focused this study on solvent effects to reflect FLT behavior in the heterogeneous tissue environment. In general, the FLTs of the NIR

dyes examined do not respond significantly to changes in ion concentrations or pH within a physiological relevant range. From the *in vitro* data obtained using a number of NIR molecular probes, we have demonstrated that the different FLTs *in vivo* depend on the nature of the molecular probe. In general, dyes with longer FLT in any given solvent generally exhibited longer FLT values *in vivo*. Data analysis of FLTs in various mediums identified albumin solution as a consensus model for predicting the *in vivo* FLT relative to the other mediums. This finding is supported by the fact that cyanine dyes are rapidly opsonized by plasma proteins such as serum albumin soon after injection.[32] Thus, a majority of the FLT
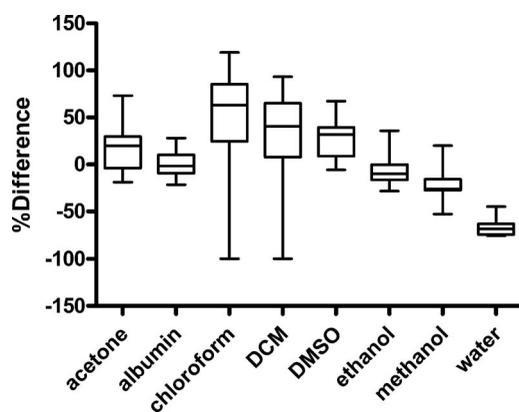

Fig. 4 Box and whiskers plot of FLTs measured in various solvents and referenced to *in vivo* data from liver regions. The mean percent difference for fluorescence lifetimes for the dyes measured in albumin solution is close to 0 (0.7%), indicating good agreement between the two systems. The maximum difference for albumin was 28% with median difference of 2%. All of the other systems showed a median difference of 10% or greater. The largest mean differences between the *in vivo* and albumin models were observed for DTTCI (28%) and LS-276 (21%). These differences appear to be related to the protein binding fractions as shown in Table 2.
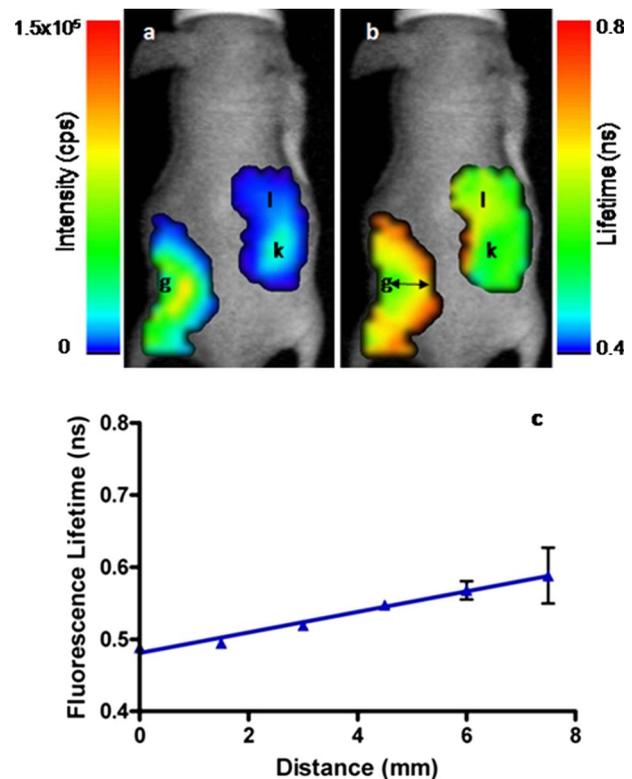
Fig. 5 (a) *In vivo* fluorescence intensity and (b) FLT maps of a mouse 3 h after subcutaneous implantation of cypate-loaded agarose gel (g). The FLT of cypate increased as it diffused through the subcutaneous space from the gel and was absorbed into the blood. Fluorescence can be seen in the right kidney (k) and the liver (l) regions, with distinctly different FLTs consistent with the dye environment. (b) A plot of FLT at distances from the agarose gel (black arrows) demonstrates the difference in cypate FLT as it diffused from the gel.
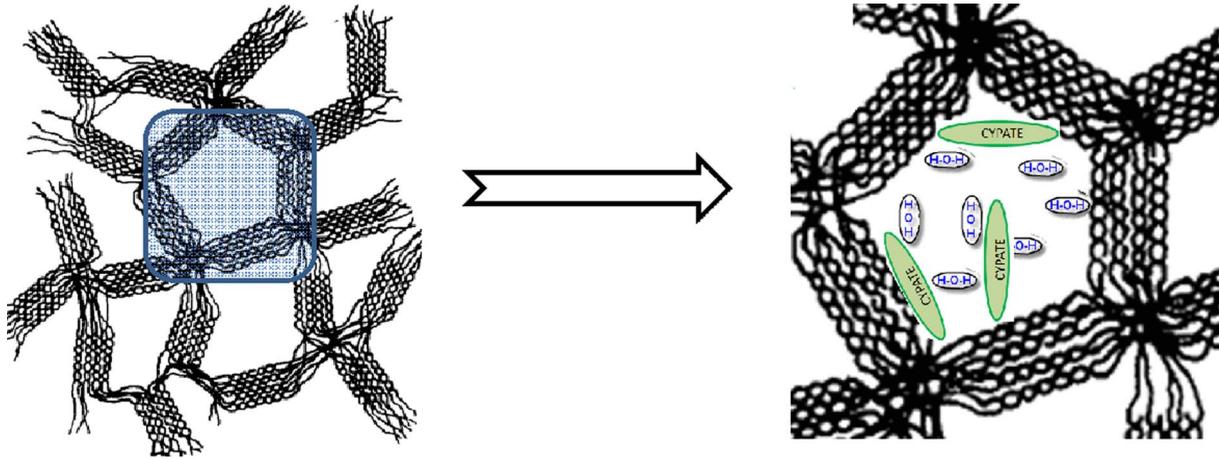
Fig. 6 3-D gel structure of agarose (adapted with permission from the *Journal of Molocular Biology*).[33] Microcavities are filled with water molecules (more than 99% of the mass of the gel is water).

values observed *in vivo* reflected the FLT of NIR dyes bound to serum albumin. In a two-component analysis, this correlation could be extended to a FLT polarity scale, where the longest and shortest FLTs observed *in vivo* correlate with FLTs of the NIR dyes bound to albumin and in water, respectively. An interesting finding is the difference in the FLT of albumin-bound (liver) versus albumin-free (bladder) NIR dye, LS 288 (Fig. 3). In the hydrophilic bladder, the FLT (0.70 ns) is between that of water and methanol, but the FLT in the liver is comparable to a value between ethanol and DMSO (Table 1). Comparison of the albumin/liver FLT to that of relatively protein-free urine (Table 3) suggests that the glomerular filtration mechanism of the kidney actively stripped the albumin of the dye, thereby excreting the free hydrophilic dye into the urine. A similar observation was not found for the relatively lipophilic dyes used in this study, which were excreted predominantly in the liver. The possible effect of the DMSO formulation on the *in vivo* FLT of dyes was not evaluated but based on other studies; this effect is expected to be negligible.

To further illustrate the utility of FLT imaging for monitoring controlled dye release *in vivo*, agarose gels containing cypate were subcutaneously implanted in the flank region of nude mice. As we descried previously, the FLT of cypate is sensitive to differences in medium polarity but less sensitive to its viscosity.[16] Thus the short FLT of cypate inside the gel (0.3 ns) reflects the presence of a large amount of water molecules trapped inside the bundles of double helices formed by agarose molecules upon gelation.[33] Indeed, this value is close to the FLT of cypate in water (0.2 ns). The slightly larger FLT value in the gel than in pure water indicates the small contribution of viscosity, or reflects a modification of the water polarity due to self-assembling of trapped water molecules inside the gel microcavities (Fig. 6).[34]

The FLT imaging showed that cypate diffuses out of the agarose gel into the more lipophilic subcutaneous space, where it is absorbed into the systemic circulation and bound by plasma proteins, specifically albumin. Further, through a cascade of biological events, the albumin released the dye to the kidneys, which subsequently drained to the bladder. These physiological processes are reflected in the progressive FLT decrease from the liver and circulating blood to the water-rich environment of the kidneys and the bladder, which is similar to the aqueous interior of the gel. The linearity of the FLT increase with distance from the gel center is likely due to the diffuse nature of optical sampling, smoothing the expected exponential diffusion function. Each pixel represents a diffuse spectroscopic measurement that includes the 3-mm region separating the source and detector. These results show that the release and delivery of fluorescent agents from implanted controlled drug release devices can be assessed by FLT imaging. The status of regional tissue physiology may also be investigated noninvasively with FLT-sensitive fluorescent probes that are administered systemically. Therefore, the FLT map complements the fluorescence intensity image by providing functional and quantifiable information about tissue physiology. FLT contrast can also aid optical imaging methods by improving 3-D localization.[11,31,35]

5 Conclusion

FLT imaging adds complimentary information to contrast-enhanced fluorescence intensity imaging. Using a number of NIR FLT-sensitive fluorescent probes in different solvents, we establish a scale that is useful for evaluation of biological events derived from *in vivo* FLT imaging. In the case of polymethine probes, the scale is based on polarity functions of the surrounding media. The shortest FLT maps *in vivo* reflect the areas with highest polarities similar to water, while the long FLTs correspond to more hydrophobic environments, mostly due to uptake by hydrophobic pockets of plasma proteins. We show that the longest FLT *in vivo* correlates with the FLT in albumin rather than to any other solvents. The use of organic and aqueous mediums to predict *in vivo* FLTs of dyes will facilitate the evaluation of new NIR dyes by the *in vitro* method, thus reducing the number of animals needed to screen agents for full characterization of biological utility. To illustrate the utility of the developed FLT scale, we image the release of cypate from agarose gel to assess the feasibility of using FLT maps for modeling controlled release of drugs and contrast agents. The results show that the mean FLT of cypate substantially increases as the dye diffuses from the gel interior to the surrounding tissue, indicating the change in the dye

environment from a highly polar gel core to the less polar tissue compartments of plasma proteins, and subsequently to hydrophilic aqueous pockets of the kidneys and urine. The results show that some biological events not available from fluorescent intensity images can be monitored directly from the FLT map. This study illustrates the potential of using FLT imaging to monitor physiological processes at different parts of the body, and opens many other opportunities in optical imaging.

Acknowledgments

References

1. V. Ntziachristos, "Fluorescence molecular imaging," *Annu. Rev. Biomed. Eng.* **8**, 1–33 (2006).
2. D. Elson, J. Requejo-Isidro, I. Munro, F. Reavell, J. Siegel, K. Suhling, P. Tadrous, R. Benninger, P. Lanigan, J. McGinty, C. Talbot, B. Treanor, S. Webb, A. Sandison, A. Wallace, D. Davis, J. Lever, M. Neil, D. Phillips, G. Stamp, and P. French, "Time-domain fluorescence lifetime imaging applied to biological tissue," *Photochem. Photobiol. Sci.* **3**(8), 795–801 (2004).
3. K. Suhling, P. M. French, and D. Phillips, "Time-resolved fluorescence microscopy," *Photochem. Photobiol. Sci.* **4**(1), 13–22 (2005).
4. P. J. Tadrous, "Methods for imaging the structure and function of living tissues and cells: 2. Fluorescence lifetime imaging," *J. Pathol.* **191**(3), 229–234 (2000).
5. A. E. Cerussi, J. S. Maier, S. Fantini, M. A. Franceschini, W. W. Mantulin, and E. Gratton, "Experimental verification of a theory for the time-resolved fluorescence spectroscopy of thick tissues," *Appl. Opt.* **36**(1), 116–124 (1997).
6. E. Kuwana and E. M. Sevick-Muraca, "Fluorescence lifetime spectroscopy in multiply scattering media with dyes exhibiting multiexponential decay kinetics," *Biophys. J.* **83**(2), 1165–1176 (2002).
7. V. Ntziachristos and R. Weissleder, "Charge-coupled-device based scanner for tomography of fluorescent near-infrared probes in turbid media," *Med. Phys.* **29**(5), 803–809 (2002).
8. J. R. Lakowicz, H. Szmacinski, K. Nowaczyk, and M. L. Johnson, "Fluorescence lifetime imaging of free and protein-bound NADH," *Proc. Natl. Acad. Sci. U.S.A.* **89**(4), 1271–1275 (1992).
9. W. Akers, F. Lesage, D. Holten, and S. Achilefu, "*In vivo* resolution of multiexponential decays of multiple near-infrared molecular probes by fluorescence lifetime-gated whole-body time-resolved diffuse optical imaging," *Mol. Imaging* **6**(4), 237–246 (2007).
10. S. Bloch, F. Lesage, L. McIntosh, A. Gandjbakhche, K. Liang, and S. Achilefu, "Whole-body fluorescence lifetime imaging of a tumor-targeted near-infrared molecular probe in mice," *J. Biomed. Opt.* **10**(5), 54003 (2005).
11. A. Godavarty, E. M. Sevick-Muraca, and M. J. Eppstein, "Three-dimensional fluorescence lifetime tomography," *Med. Phys.* **32**(4), 992–1000 (2005).
12. M. Hassan, J. Riley, V. Chernomordik, P. Smith, R. Pursley, S. B. Lee, J. Capala, and A. H. Gandjbakhche, "Fluorescence lifetime imaging system for *in vivo* studies," *Mol. Imaging* **6**(4), 229–236 (2007).
13. R. E. Nothdurft, S. V. Patwardhan, W. J. Akers, S. Achilefu, and J. P. Culver, "Fluorescence lifetime tomography for whole body small animal imaging," in *Biomedical Optics/Digital Holography and Three-Dimensional Imaging/Laser Applications to Chemical, Security and Environmental Analysis on CD-ROM*, BWE2, The Optical Society of America, Washington, DC (2008).
14. A. Abulrob, E. Brunette, J. Slinn, E. Baumann, and D. Stanimirovic, "*In vivo* time domain optical imaging of renal ischemia-reperfusion injury: discrimination based on fluorescence lifetime," *Mol. Imaging* **6**(5), 304–314 (2007).
15. J. S. Reynolds, T. L. Troy, R. H. Mayer, A. B. Thompson, D. J. Waters, K. K. Cornell, P. W. Snyder, and E. M. Sevick-Muraca, "Imaging of spontaneous canine mammary tumors using fluorescent contrast agents," *Photochem. Photobiol.* **70**(1), 87–94 (1999).
16. M. Y. Berezin, H. Lee, W. Akers, and S. Achilefu, "Near infrared dyes as lifetime solvatochromic probes for micropolarity measurements of biological systems," *Biophys. J.* **93**(8), 2892–2899 (2007).
17. S. Achilefu, R. B. Dorshow, J. E. Bugaj, and R. Rajagopalan, "Novel receptor-targeted fluorescent contrast agents for in vivo tumor imaging," *Invest. Radiol.* **35**(8), 479–485 (2000).
18. H. Lee, J. C. Mason, and S. Achilefu, "Heptamethine cyanine dyes with a robust C-C bond at the central position of the chromophore," *J. Org. Chem.* **71**(20), 7862–7865 (2006).
19. J. C. Mason, "The synthesis of novel near-infrared heptamethine cyanine dyes," in *Chemistry*, Georgia State University, Atlanta, GA (2001).
20. M. Y. Berezin, H. Lee, W. Akers, G. Nikiforovich, and S. Achilefu, "Ratiometric analysis of fluorescence lifetime for probing binding sites in albumin with near-infrared fluorescent molecular probes," *Photochem. Photobiol.* **83**, 1–8 (2007).
21. A. Yodh and B. Chance, "Spectroscopy and Imaging with Diffusing Light," *Phys. Today* **48**(3), 34–40 (1995).
22. Y. Ye, W. P. Li, C. J. Anderson, J. Kao, G. V. Nikiforovich, and S. Achilefu, "Synthesis and characterization of a macrocyclic near-infrared optical scaffold," *J. Am. Chem. Soc.* **125**(26), 7766–7767 (2003).
23. K. Dowling, M. J. Dayel, M. J. Lever, P. M. French, J. D. Hares, and A. K. Dymoke-Bradshaw, "Fluorescence lifetime imaging with picosecond resolution for biomedical applications," *Opt. Lett.* **23**(10), 810–812 (1998).
24. R. Cubeddu, G. Canti, A. Pifferi, P. Taroni, and G. Valentini, "Fluorescence lifetime imaging of experimental tumors in hematoporphyrin derivative-sensitized mice," *Photochem. Photobiol.* **66**(2), 229–236 (1997).
25. R. Cubeddu, G. Canti, P. Taroni, and G. Valentini, "Time-gated fluorescence imaging for the diagnosis of tumors in a murine model," *Photochem. Photobiol.* **57**(3), 480–485 (1993).
26. J. R. Lakowicz, H. Szmacinski, K. Nowaczyk, K. W. Berndt, and M. Johnson, "Fluorescence lifetime imaging," *Anal. Biochem.* **202**(2), 316–330 (1992).
27. P. J. Tadrous, J. Siegel, P. M. French, S. Shousha, N. Lalaniel, and G. W. Stamp, "Fluorescence lifetime imaging of unstained tissues: early results in human breast cancer," *J. Pathol.* **199**(3), 309–317 (2003).
28. S. Andersson-Engels, G. Canti, R. Cubeddu, C. Eker, C. af Klinteberg, A. Pifferi, K. Svanberg, S. Svanberg, P. Taroni, G. Valentini, and I. Wang, "Preliminary evaluation of two fluorescence imaging methods for the detection and the delineation of basal cell carcinomas of the skin," *Lasers Surg. Med.* **26**(1), 76–82 (2000).
29. A. H. Gandjbakhche, V. Chernomordik, D. Hattery, M. Hassan, and I. Gannot, "Tissue characterization by quantitative optical imaging methods," *Technol. Cancer Res. Treat.* **2**(6), 537–551 (2003).
30. D. Schweitzer, M. Hammer, F. Schweitzer, R. Anders, T. Doebbecke, S. Schenke, E. R. Gaillard, and E. R. Gaillard, "In vivo measurement of time-resolved autofluorescence at the human fundus," *J. Biomed. Opt.* **9**(6), 1214–1222 (2004).
31. A. T. N. Kumar, S. B. Raymond, G. Boverman, D. A. Boas, and B. J. Bacskai, "Time resolved fluorescence tomography of turbid media based on lifetime contrast," *Opt. Express* **14**(25), 12255–12270 (2006).
32. G. R. Cherrick, S. W. Stein, C. M. Leevy, and C. S. Davidson, "Indocyanine green: observations on its physical properties, plasma decay, and hepatic extraction," *J. Clin. Invest.* **39**, 592–600 (1960).
33. S. Arnott, A. Fulmer, W. E. Scott, I. C. M. Dea, R. Moorhouse, and D. A. Rees, "The agarose double helix and its function in agarose gel structure," *J. Mol. Biol.* **90**(2), 269–272 (1974).
34. B. Ratajska-Gadomska and W. Gadomski, "Water structure in nanopores of agarose gel by Raman spectroscopy," *J. Chem. Phys.* **121**(24), 12583–12588 (2004).
35. D. Hall, G. Ma, F. Lesage, and Y. Wang, "Simple time-domain optical method for estimating the depth and concentration of a fluorescent inclusion in a turbid medium," *Opt. Lett.* **29**(19), 2258–2260 (2004).